

# Short hairpin RNA attenuates liver fibrosis by regulating the PPAR- $\gamma$ and NF- $\kappa$ B pathways in HBV-induced liver fibrosis in mice

LEI YE<sup>1\*</sup>, TING CHEN<sup>1\*</sup>, JIAQI CAO<sup>1</sup>, LIYING SUN<sup>1</sup>, WUPING LI<sup>1</sup> and CHENGHAI ZHANG<sup>2</sup>

<sup>1</sup>NHC Key Laboratory of Systems Biology of Pathogens (Institute of Pathogen Biology, Chinese Academy of Medical Sciences and Peking Union Medical College), Beijing 100730; <sup>2</sup>Shanghai Mabgeek Biotech. Co., Ltd., Shanghai 201203, P.R. China

Received December 11, 2019; Accepted August 27, 2020

DOI: 10.3892/ijo.2020.5125

**Abstract.** Progressive liver fibrosis, caused by chronic viral infection and metabolic disorders, results in the development of cirrhosis and hepatocellular carcinoma. However, no antifibrotic therapies have been approved to date. In our previous study, adeno-associated virus (AAV) short hairpin RNAs (shRNAs) targeting hepatitis B virus (HBV) and transforming growth factor (TGF)- $\beta$  administration could persistently inhibit HBV replication and concomitantly prevent liver fibrosis. However, the differentially expressed

proteins and critical regulatory networks of AAV-shRNA treatment remain unclear. Accordingly, in the present study, we aimed to analyze differentially expressed proteins in the liver of AAV-shRNA-treated mice with HBV infection and liver fibrosis using isobaric tags for relative and absolute quantitation (iTRAQ)-based quantitative proteomics and to elucidate the underlying antifibrotic mechanisms. In total 2,743 proteins were recognized by iTRAQ-based quantitative proteomics analysis. Gene Ontology analysis revealed that the differentially expressed proteins mostly participated in peptide metabolism in the biological process category, cytosolic ribosomes in the cell component category, and structural constituents of ribosomes in the molecular function category. Kyoto Encyclopedia of Genes and Genomes pathway analysis indicated that oxidative stress and the peroxisome proliferator-activated receptor (PPAR) signaling pathway were activated after treatment. Verification studies revealed that AAV-shRNAs inhibited hepatic stellate cell activation and inflammation by suppressing nuclear factor- $\kappa$ B p65 phosphorylation and  $\alpha$ -smooth muscle actin expression via upregulation of PPAR- $\gamma$ . Hepatocytes steatosis was also decreased by activating the PPAR signaling pathway and improving lipid metabolism. The expression level of TGF- $\beta$  was decreased due to upregulation of PPAR- $\gamma$  expression and direct inhibition using AAV-shRNA targeting TGF- $\beta$ . TGF- $\beta$ -induced oxidative stress was suppressed by increasing glutathione S-transferase Pi 1 and reducing peroxiredoxin 1. Collectively, the present results indicated that AAV-shRNAs were effective in modulating liver fibrosis by reducing oxidative stress, inflammation and activating the PPAR signaling pathway.

*Correspondence to:* Dr Wuping Li, NHC Key Laboratory of Systems Biology of Pathogens (Institute of Pathogen Biology, Chinese Academy of Medical Sciences and Peking Union Medical College), 9 Dong Dan San Tiao, Beijing 100730, P.R. China  
E-mail: liwuping@ipbcams.ac.cn

Dr Chenghai Zhang, Shanghai Mabgeek Biotech. Co., Ltd., 1011 Harley Road, Shanghai 201203, P.R. China  
E-mail: chenghai.zhang@mabgeek.com

*Abbreviations:* AAV, adeno-associated virus; shRNA, short hairpin RNA; HBV, hepatitis B virus; TGF, transforming growth factor; iTRAQ, isobaric tags for relative and absolute quantitation; PPAR, peroxisome proliferator-activated receptor; ROS, reactive oxygen species; NF- $\kappa$ B, nuclear factor- $\kappa$ B; GO, Gene ontology; KEGG, Kyoto Encyclopedia of Genes and Genomes; CC, cell component; MF, molecular function; BP, biological process; TRAF2-GSTP1, tumor necrosis factor receptor-associated factor 2-glutathione S-transferase Pi; PPI, protein-protein interaction; GSTP1, glutathione S-transferase Pi 1; Rpl, ribosome large subunit protein; FABP1, fatty acid binding protein 1; ME1, malic enzyme 1; ACAA1, acetyl-CoA acyltransferase 1; PRDX1, peroxiredoxin-1; LC-MS/MS, liquid chromatography-mass spectrometry/mass spectrometry

\*Contributed equally

*Key words:* quantitative proteomics, oxidative stress, peroxisome proliferator-activated receptor signaling pathway, nuclear factor- $\kappa$ B, liver fibrosis

## Introduction

Hepatitis B virus (HBV) infection is a major health problem, which causes acute and chronic hepatitis, and progresses to cirrhosis, and hepatocellular carcinoma (HCC) (1-4). More than 800,000 people succumb to HBV infection or related complications each year (5). Approximately 25-40% of cases of liver fibrosis result in cirrhosis or HCC (6,7). Moreover 70-90% of clinical HCC cases are related to advanced liver fibrosis or cirrhosis (8).

Liver fibrosis is a common wound healing process response to chronic liver injury via excessive production and deposition of extracellular matrix (ECM) (9). Hepatic stellate cells (HSCs) are major producers of matrix components and play pivotal roles in regulating the production and secretion of the ECM (10). Typically, HSCs remain in a quiescent state and function in the storage of vitamin A. Upon liver injury, HSCs may undergo transdifferentiation, transform into highly proliferative myofibroblast-like cells, and acquire fibrogenic properties, including expression of  $\alpha$ -smooth muscle actin ( $\alpha$ -SMA), type I collagen, and type III collagen, which are vital components of the ECM (11). Although inhibition of HSC activation has been proposed as a therapeutic strategy in anti-fibrosis treatment of fibrosis (12), novel approaches to reveal the mechanisms of liver fibrosis and for the development of antifibrotic treatments remain challenging.

Transforming growth factor (TGF)- $\beta$  is a critical mediator that plays important roles in human fibrogenesis (13). Numerous studies have revealed that TGF- $\beta$  signaling through the Smad pathway and reactive oxygen (ROS) imbalance are responsible for liver fibrosis (14-17). TGF- $\beta$  has also been revealed to inhibit the antioxidant system and hence induce oxidative stress or redox imbalance (18-20). Redox imbalance has been revealed to significantly contribute to TGF- $\beta$ -related fibrosis (16). Therapeutics targeting TGF- $\beta$ -induced ROS-dependent cellular signaling may be a new therapeutic method in the treatment of fibrotic disorders. However, the mechanisms underlying liver fibrosis associated with redox-sensitive targets remain unclear.

Peroxisome proliferator activated receptors (PPARs) including PPAR- $\alpha$ , PPAR- $\beta/\delta$ , and PPAR- $\gamma$ , are ligand-activated transcription factors belonging to the nuclear hormone receptor family (21-25). Previous studies have revealed that PPAR- $\gamma$  is predominantly present in adipose tissue, and plays an important role in numerous biological processes, such as adipogenesis, cell differentiation, cell growth regulation and inflammatory reactions (26,27). Activation of PPAR- $\gamma$  has been revealed to retard the progression of liver fibrosis, and its activation promotes insulin sensitivity and inhibits the transformation of HSCs from a quiescent to activated state (28-31). Previous studies have indicated that the activation of PPAR- $\gamma$  can reduce connective tissue growth factor expression induced by TGF- $\beta$ 1 in HSCs (32) and that the PPAR- $\gamma$  agonist rosiglitazone can enhance PPAR- $\gamma$  expression in activated HSCs, leading to reduced oxidative stress and decreased expression of  $\alpha$ -SMA and collagen I (33).

The transcriptional regulator nuclear factor (NF)- $\kappa$ B is an important mediator of inflammatory signals in response to stimulation (34-36). Numerous studies have revealed that upregulation of NF- $\kappa$ B stimulates HSC proliferation and inhibits HSC apoptosis, playing a key role in fibrogenesis (36-38). Moreover, NF- $\kappa$ B can induce the expression of inflammatory factors [TGF- $\beta$ , interleukin (IL)-6, and tumor necrosis factor- $\alpha$ ], which play pivotal roles in the development of liver fibrosis (36,37,39,40). Excessive production of ROS also can induce phosphorylation of NF- $\kappa$ B, which then migrates to the nucleus to increase the transcription of pro-inflammatory cytokines and results in HSC activation (41). Accordingly, reducing the activation of NF- $\kappa$ B can lead to inhibition of HSC activation and ECM production (42,43).

Recent studies have revealed numerous mechanisms that mediate liver fibrosis. However, no highly effective antifibrotic therapies are currently available. In our previous study, we found that adeno-associated virus (AAV) short hairpin RNAs (shRNAs) targeting HBV and TGF- $\beta$  inhibited HBV replication and liver fibrosis in an HBV-induced liver fibrosis mouse model (44). Removal of the causative agent (HBV) by RNA interference (RNAi) was an effective strategy for treating HBV-induced liver fibrosis, whereas inhibition of the TGF- $\beta$  pathway alone was not effective. Our previous studies revealed the advantages of the combinatorial use of shRNAs against both HBV and TGF- $\beta$  in alleviating liver fibrosis (44,45). The mechanisms through which RNAi protects against HBV are unclear, and the inhibiting or activating responses of host factors remain elusive. Isobaric tags for relative and absolute quantification (iTRAQ) has been widely applied to identify differentially expressed proteins in numerous diseases (46-48) including liver fibrosis (49,50). As a potent new technique in comparative proteomics analysis, iTRAQ has relatively high sensitivity and allows the determination of diverse proteins compared with traditional proteome approaches (51).

In the present study, liver proteins were analyzed in AAV-shRNA-treated mice using iTRAQ-based quantitative proteomics in order to identify differentially expressed proteins and to elucidate the therapeutic mechanisms of liver fibrosis.

## Materials and methods

**Animal study.** Nine normal C57BL/6 male mice (aged 6-8 weeks; weighing 16-18 g; Beijing Vital River Laboratory Animal Technology Co., Ltd.) were housed and maintained at the Laboratory Animal Facility of the Institute of Laboratory Animal Sciences, Chinese Academy of Medical Sciences. The protocols for the care and use of laboratory animals were approved by the Institutional Animal Care and Use Committee of the Chinese Academy of Medical Sciences, and all animal care procedures and experiments were performed in accordance with these protocols. Briefly, mice were housed at room temperature (20-25°C) and relative humidity (45-60%) with a 12-h light/dark cycle under individually ventilated cage (IVC) systems. AAV8-HBV1.2 vector [2x10<sup>11</sup> vector genome (vg) equivalents] was injected into mice via the tail vein to construct an HBV persistent replication model as previously described (44,52). Serum samples were obtained by collection of blood from the tail vein into heparinized capillary tubes using standard methods 1 month after injection and then subjected to enzyme-linked immunosorbent assays (ELISAs) and quantitative polymerase chain reaction (qPCR). After dilution with PBS, the serum HBV surface antigen (HBsAg) and HBV e antigen (HBeAg) concentrations were measured using an Auszyme Monoclonal Diagnostic ELISA kit according to the manufacturer's instructions (Abbott Laboratories). Serum or cellular DNA was extracted using DNeasy Blood and Tissue Kits (Invitrogen; Thermo Fisher Scientific, Inc.) according to the manufacturer's instructions and stored at -80°C prior to PCR analyses.

Total RNA was isolated using a NucleoSpinRNA II kit (Macherey Nagal, GmbH & Co., KG) and reverse transcribed using a First Strand cDNA Synthesis Kit (Toyobo Life Science). A qPCR standard curve was generated using 10-fold dilutions of the SSV9-1.2HBV plasmid (1.0x10<sup>3</sup>-1.0x10<sup>9</sup> copies/ml). All

of the qPCR reactions were performed in triplicate in 96-well optical reaction plates using an ABI 7900 Sequence Detection System (Applied Biosystems; Thermo Fisher Scientific, Inc.) and SYBR Green I PCR mix (Roche Diagnostics) as previously described (52). PCR was performed under the following conditions: One cycle at 95°C for 10 min; 40 cycles at 95°C for 15 sec, 55°C for 30 sec, and 72°C for 30 sec and then a dissolution curve was produced.

HBsAg-, HBeAg- and HBV DNA-positive mice were injected with AAV-shRNA1+3 and AAV-shRNA-TGF- $\beta$ , or AAV-scrambler ( $2 \times 10^{11}$  vg), respectively. Normal C57BL/6 mice were injected with phosphate-buffered saline (PBS) as a negative control and designated as HBV(-) mice. HBV-positive mice were injected with AAV-scrambler and designated as HBV(+) mice. AAV-shRNA1+3 targeted S and X coding regions of HBV. AAV-shRNA-TGF- $\beta$  vectors targeted the coding region of TGF- $\beta$ . The AAV vector containing the shRNA sequence not targeted to the HBV genome was designated as AAV-scrambler as previously described (44). All mice were sacrificed at 6 months after injection. Serum and liver samples were collected and frozen at -80°C in a freezer or liquid nitrogen. All shRNA sequences targeting HBV and TGF- $\beta$  are listed Table SI.

At the end of the experiment, mice were anesthetized with 2.5% avertin and perfused with cold PBS (pH 7.4) transcardially, followed by 4% paraformaldehyde (over 2 h at 25°C) in PBS (0.1 M, pH 7.4) (Boster Biological Technology Co., Ltd.) to fix tissues for immunohistochemistry (IHC). Livers were then collected for IHC analysis. Intrahepatic HBV core antigen (HBcAg) and HBsAg were evaluated by IHC staining of paraffin-embedded tissues (6- $\mu$ m thickness of sections) incubated with rabbit anti-HBc (1:100 dilution; product code ab115992; Abcam) and goat anti-HBs antibodies (1:200 dilution; cat. no. PA1-73084, Thermo Fisher Scientific, Inc.), respectively, at 37°C and 45 min and developed with the Envision HRP (diaminobenzidine) system (Dako; Agilent Technologies, Inc.). Liver sections were examined with light microscopy after Masson's trichrome staining and Sirius Red staining (scale bar, 250  $\mu$ m). Sirius red staining of liver sections was also observed by polarizing microscope (scale bar, 250  $\mu$ m). Total collagen in the liver was determined using a Hydroxyproline Colorimetric Assay Kit according to the manufacturer's instructions (BioVison, Inc.). Image-Pro Plus software 6.0 supplied by Media Cybernetics, Inc. was used for analysis.

**Treatment groups.** The various treatment groups were as follows: Treated mice, HBV-positive mice were infected with AAV-shRNA1+3 and AAV-shRNA-TGF- $\beta$ ; AAV-shRNA1+3, the combination of two shRNAs against S and X coding regions of HBV by a self-complementary AAV vector; AAV-shRNA-TGF- $\beta$ , vector carrying shRNA against TGF- $\beta$ ; HBV(+) mice, HBV-positive mice were infected with AAV-scrambler; AAV-scrambler, AAV vector containing shRNA sequence not targeted to the HBV genome; HBV(-) mice, normal mice were injected with PBS; AAV-shRNA-treated mice, treated mice.

**Protein preparation and iTRAQ labeling.** Total protein extraction was performed using a kit (FOCUS Mammalian Proteome; G-Biosciences) in accordance with the

manufacturer's instructions. Protein samples were stored at -80°C for proteomic analysis and western blotting. The iTRAQ method used was previously described (53). Briefly, total protein concentrations were determined using an EZQ Protein Quantitation Kit (Invitrogen; Thermo Fisher Scientific, Inc.), and protein samples from treated mice, HBV(+) mice and HBV(-) mice were reconstituted in dissolution buffer, denatured, reduced, and trypsinized. Next, tryptic digests of the samples were labeled with iTRAQ reagents (Table SII). All samples were balanced, mixed, and pre-separated for liquid chromatography (LC)-mass spectrometry (MS)/MS analysis.

**Nano-LC-MS/MS analysis.** LC-MS/MS analysis was performed with an Easy-nLC1000 (Thermo Fisher Scientific, Inc.) and Q Exactive MS (Thermo Fisher Scientific, Inc.). A reversed-phase ReproSil-PurC18-AQ column (column, 3  $\mu$ m; 120 Å, 100  $\mu$ m x 10 cm) was used to separate the peptides at a flow rate of 600 nL/min. The LC linear gradient elution was performed from 6 to 9% B (0.1% formic acid in acetonitrile) for 15 min, 9 to 14% B for 20 min, 14 to 30% B for 60 min, 30 to 40% B for 15 min, and 40 to 95% B for 3 min, followed by elution with 95% B for 7 min. A precursor scan was performed using an Orbitrap instrument by scanning from m/z 300-1800 for detection with Q Exactive MS. The MS resolution was 60,000 at 400 m/z. The parameters of MS/MS settings were as follows: The product ion scan range started at 100 m/z; the activation type was collision-induced dissociation (CID); the minimum signal required was 1500; the isolation width was 3; the normalized collision energy was 40; the default charge state was 6; the activation Q was 0.25; the activation time was 30 sec. Data were acquired using a data-dependent acquisition mode in which, for each cycle, the most abundant multiply-charged peptides with an m/z between 300 and 1800 were selected for MS/MS with the 15 sec dynamic exclusion setting.

**Functional analysis of differentially expressed proteins.** In order to reduce false positives of differentially expressed proteins, an additional cut off of fold change greater than 1.30 or less than 0.77 (1/1.3) was exploited for all iTRAQ ratios (54). Proteins with iTRAQ ratios >1.30 or <0.77 were considered upregulated or downregulated, respectively. Gene Ontology (GO) annotations (46,55), pathway enrichment, and protein-protein interaction (PPI) networks for all the identified proteins and differentially expressed proteins were evaluated with OmicsBean (<http://www.omicsbean.cn>). GO annotations were classified into three major categories, including biological processes (BPs), cell components (CCs), and molecular functions (MFs). Pathway enrichment analysis was performed with Kyoto Encyclopedia of Genes and Genomes (KEGG) mapping (47,49). PPI networks were applied to obtain key nodes, such as degree centrality, betweenness, closeness, and cluster coefficient and Venn diagrams were used to reveal mathematical or logical associations between the HBV(+) vs. HBV(-) groups and the treated vs. HBV(+) groups.

**Immunoblotting.** For immunoblotting, 10  $\mu$ g protein from liver tissue was separated by sodium dodecyl sulfate polyacrylamide gel electrophoresis (SDS-PAGE) on 4-12% gels. The separated proteins were blotted onto polyvinylidene difluoride membranes, and the membranes were then

Table I. Baseline characteristics of mice used in this study.

Mice	Sex (Male/Female)	HBsAg serum (IU/ml)	HBV-DNA serum (copies/ml)	HBV-DNA liver (copies/g)	Collagen liver ( $\mu$ g/mg)	Collagen I serum (pg/ml)	Collagen III serum (pg/ml)
Treated	M	125.80	1.80x10 <sup>4</sup>	2.01x10 <sup>8</sup>	107.48	141.34	0.51
N=3	M	383.70	2.51x10 <sup>4</sup>	2.00x10 <sup>8</sup>	112.24	159.45	0.75
	M	0.40	1.04x10 <sup>4</sup>	1.60x10 <sup>8</sup>	104.55	143.51	0.62
HBV(+)	M	>2,500.00	1.70x10 <sup>5</sup>	2.15x10 <sup>8</sup>	241.29	332.12	1.31
N=3	M	>2,500.00	4.24x10 <sup>4</sup>	4.81x10 <sup>8</sup>	236.29	349.49	1.45
	M	>2,500.00	5.02x10 <sup>4</sup>	5.01x10 <sup>8</sup>	375.75	365.75	1.75
HBV(-)	M	-	-	-	95.50	131.14	0.30
N=3	M	-	-	-	100.21	145.49	0.52
	M	-	-	-	94.01	132.42	0.27

Treated mice, HBV-positive mice were infected with AAV-shRNA1+3 and AAV-shRNA-TGF- $\beta$ . AAV-shRNA1+3 targeting S and X coding regions of HBV, and AAV-shRNA-TGF- $\beta$  targeting the TGF- $\beta$  coding region. HBV(+) mice, HBV-positive mice were infected with AAV-scrambler. AAV-scrambler, AAV vector containing shRNA sequence not targeted to the HBV genome. HBV(-) mice, normal mice were injected with PBS. HBV, hepatitis B virus. AAV, adeno-associated virus; shRNA, short hairpin RNA; TGF, transforming growth factor.

washed with TBST and then incubated with blocking buffer containing 5% skimmed milk in TBST for 2 h at 25°C. The membranes were washed again with TBST and incubated overnight at 4°C with primary antibodies diluted in TBST. The primary antibodies were rabbit anti-mouse antibodies targeting glutathione S-transferase Pi 1 (GSTP1; 1:2,000 dilution; cat. no. 15902-1-AP), peroxiredoxin-1 (PRDX1; 1:10,000 dilution; cat. no. 15816-1-AP), acetyl-CoA acyltransferase 1 (ACAA1; 1:1,000 dilution; cat. no. 12319-2-AP), malic enzyme 1 (ME1; 1:2,000 dilution; cat. no. 16619-1-AP), fatty acid binding protein 1 (FABP1; 1:1,000 dilution; cat. no. 13626-1-AP), PPAR- $\alpha$  (1:500 dilution; cat. no. 15540-1-AP) and PPAR- $\gamma$  (1:1,000 dilution; cat. no. 16643-1-AP) (all from ProteinTech Group),  $\alpha$ -SMA (1:4,000 dilution; product code ab124964; Abcam), TGF- $\beta$  (1:1,000 dilution; cat. no. 21898-1-AP; ProteinTech Group), NF- $\kappa$ B p65 (1:1,000 dilution; product no. 8242), and phospho-NF- $\kappa$ B p65 Ser468; (1:1,000 dilution; product no. 3039; both from Cell Signaling Technology, Inc.), and glyceraldehyde 3-phosphate dehydrogenase (GAPDH; 1:10,000 dilution; product code ab181602; Abcam Inc.). The membranes were then incubated with goat anti-rabbit secondary antibodies, HRP (1:10,000 dilution; cat. no. 31460; Thermo Fisher Scientific, Inc.) for 1 h at room temperature. Finally, the signal was visualized using an electrochemiluminescent reagent kit (EMD Millipore), and blots were imaged using X-ray film. ImageJ software v.1.31 was used for densitometric analysis.

**Cell line.** LX-2 cells (obtained from the Chinese Academy of Medical Sciences and Peking Union Medical College) were maintained in Dulbecco's modified Eagle's medium supplemented with 10% fetal bovine serum and 1% penicillin-streptomycin solution (all from Thermo Fisher Scientific, Inc.) at 37°C in a humidified incubator with 5% CO<sub>2</sub>. LX-2 cells were seeded into 6-well plates at 4x10<sup>5</sup> cells/well and cultured. pSSV9-HBV1.2 was transfected into LX-2 cells using Lipofectamine 2,000 (Thermo Fisher Scientific, Inc.) with or without pAAV-shRNAs

(pAAV-shRNA1+3 and pAAV-shRNA-TGF- $\beta$  or pAAV-scrambler) (3  $\mu$ g) according to the manufacturer's instructions. Lipofectamine was used as a negative control. The supernatants and transfected cells were collected 72 h after transfection and subjected to protein extraction with RIPA Lysis and Extraction Buffer (Thermo Fisher Scientific, Inc.). The concentration of protein was determined with a Thermo Scientific Pierce BCA Protein Assay Kit. Transfection efficiency was evaluated using HBsAg and HBeAg ELISA kits according to the manufacturer's instructions (Shanghai Kehua Bio-Engineering, Co., Ltd.).

**Statistical analysis.** The data are reported as the means  $\pm$  standard deviations. One-way analysis of variance (ANOVA) with GraphPad Prism 5.0 (GraphPad Software, Inc.) was used to determine statistically significant differences between groups. P-values <0.05 were considered to indicate statistically significant differences.

## Results

**Baseline characteristics of the study mice.** Our previous study demonstrated that co-administration of shRNAs targeting HBV and TGF- $\beta$  decreased HBV antigens, HBV DNA, and liver fibrosis markers in the serum and livers of HBV-replicated mice (44). In order to explore the mechanisms underlying the antiviral and antifibrotic effects, AAV-shRNA1+3 and AAV-shRNA-TGF- $\beta$  co-injection was evaluated. HBV(+) and HBV(-) mice were used as positive and negative controls, respectively. All three treated mice exhibited lower HBsAg and HBV DNA levels in the serum compared with that in untreated mice (Table I). HBsAg and HBeAg levels were significantly decreased in the livers of treated mice, as demonstrated by IHC staining (Fig. 1). The sequence of shRNAs for HBV and TGF- $\beta$  were available in supplementary Table SI.

Collagen levels were significantly decreased in the livers of treated mice compared with those in HBV(+) mice (Fig. 2A, Table I). Total collagen was also quantitatively

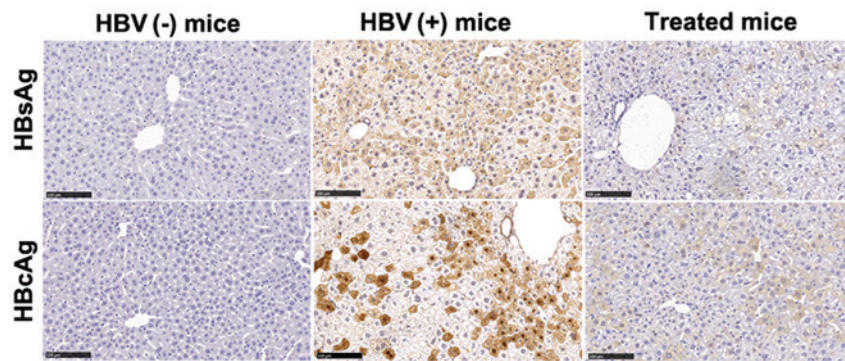


Figure 1. AAV-shRNA treatment decreases HBsAg and HbcAg in hepatocytes from HBV-replicated mice. Liver samples from mice treated with AAV-shRNAs were collected at 6 months after injection. Liver sections were fixed and stained for HBsAg and HbcAg using IHC staining. HBsAg- and HbcAg-positive hepatocytes were stained brown. Treated mice, HBV-positive mice were infected with AAV-shRNA1+3 and AAV-shRNA-TGF- $\beta$ ; HBV(+) mice, HBV-positive mice were infected with AAV-scrambler; HBV(-) mice, normal mice were injected with PBS. Scale bar, 100  $\mu$ m. Three mice were detected in each group. The representative sections are presented. AAV, adeno-associated virus; shRNA, short hairpin RNA; HBsAg, HBV surface antigen; HbcAg, HBV core antigen; HBV, hepatitis B virus; IHC, immunohistochemical.

assessed using hydroxyproline assays; lower collagen levels were observed in the livers of treated mice and HBV(-) mice than in those of HBV(+) mice (Table I). Masson staining and Sirius Red staining revealed that the percentages of collagen deposition in hepatocytes were decreased by approximately 67.71 and 80.01%, respectively, after treatment (Fig. 2B and C). Collagen I and III levels in serum were also significantly reduced in the treated group compared with that in HBV(+) mice (Table I).

Next, the expression of  $\alpha$ -SMA, a marker of fibrosis, was detected in the liver by IHC staining (Fig. 2A) and western blotting (Fig. 2D). As indicated by IHC staining,  $\alpha$ -SMA expression was markedly reduced in the treated group compared with that in the HBV(+) group (Fig. 2A). The percentage of  $\alpha$ -SMA expression was decreased by over 45% in the livers of treated mice compared with that in HBV(+) mice, as demonstrated by western blotting (Fig. 2D). Collectively, these data indicated that the mouse model in this study was appropriate.

*Proteomic analysis of AAV-shRNA-treated HBV-replicated mice by iTRAQ-based quantitative proteomics.* Next, differentially expressed proteins and potential pathways were investigated for attenuating liver fibrosis using iTRAQ-based quantitative proteomics by comparing these three groups of mice in order to elucidate the potential antifibrotic mechanisms. AAV-shRNA1+3- and AAV-shRNA-TGF- $\beta$ -treated groups were analyzed by iTRAQ-based quantitative proteomics, as revealed in the flowchart in Fig. 3A. HBV(+) mice were used as a positive control, and HBV(-) mice were used as a negative control. In total, 2,743 proteins were identified in all groups (Fig. 3B and C). Notably, 76 downregulated and 122 upregulated proteins were revealed in the treated group compared with that in the HBV(+) group (Table SIII). Sixty-one proteins were upregulated, and 134 proteins were downregulated in HBV(+) mice compared with that in HBV(-) mice (Table SIV). We also evaluated the differentially expressed proteins in all three groups using Venn-Euler diagrams (Fig. 3D) and found 41 upregulated and 15 downregulated proteins in the treated group vs. the HBV(+) group compared with the HBV(+) group vs. the HBV(-) group (Table SV). Two proteins (Abcb7 and

Chil3) were upregulated in both comparisons, and two proteins (Opa1 and Eml2) were downregulated in both comparisons (Fig. 3D; Tables SV, SVI and SVII).

In order to obtain an overall functional view of the differentially expressed proteins, GO functional annotations and KEGG metabolic pathway analyses were used. Comparison of the treated group and HBV(+) group revealed enrichment of 2,185 BPs; 321 of these BPs were significant according to analysis of P-values. Additionally, 89 CCs were significantly altered among 337 enriched CCs, and 484 MFs were enriched, among which 144 MFs were significant. Seventeen KEGG terms among 99 enriched KEGG terms were significant (Fig. 4A). In order to clarify the functions and features of the identified proteins, we annotated protein functions and features based on GO and KEGG analyses. An overview of the GO analysis is presented in Fig. 4B. There were 10 distinctly enriched categories of BPs, CCs, and MFs. The top proteins enriched in BPs were involved in organ-nitrogen compound metabolic process (45%), and some proteins enriched in BPs were related to liver fibrosis, e.g., lipid metabolic process (11%), oxidation-reduction (11%), response to oxidative stress (5%), negative regulation of cell adhesion (4%), and cellular oxidant detoxification (2%; Fig. S1A). The main MF category of enriched proteins was cytoplasm (85%). Proteins involved in hepatic fibrosis and oxidative stress were also observed in MFs, including adherens junction (7%), endoplasmic reticulum membrane (7%), complex of collagen trimers (2%), and the TRAF2-GSTP1 complex (1%; Fig. S1B). Proteins enriched in CCs were involved in nucleic acid binding (40%), hydrolase activity (8%), oxidoreductase activity (4%), organic acid binding (3%), transferase activity (3%), vitamin binding (2%), and vitamin B6 binding (2%; Fig. S1C).

These proteins were also mapped to KEGG pathways based on their KEGG gene IDs. There were seventeen significant KEGG pathways presented, including metabolic pathways (14%), ribosome (13%), PPAR signaling pathway (6%), chemical carcinogenesis (3%), protein digestion and absorption (2%), protein export (1%), tryptophan metabolism (2%), and valine, leucine, and isoleucine degradation (2%; Fig. 4C). The significant ( $P < 0.05$ ) pathways were ribosome, PPAR signaling pathway, and chemical carcinogenesis (Fig. S2A).

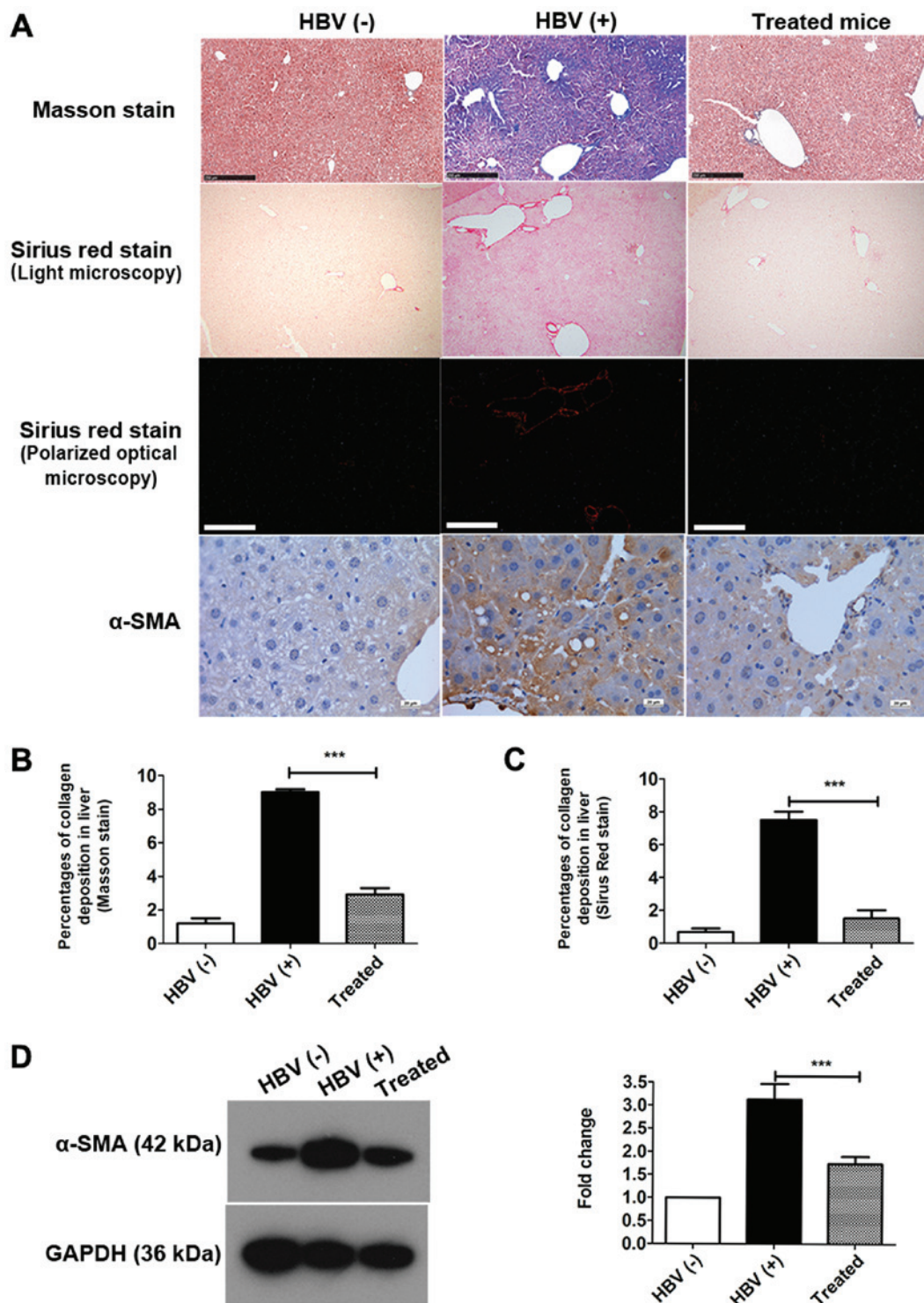


Figure 2. AAV-shRNA treatment attenuates collagen deposition and liver fibrosis in HBV-replicated mice. Mice received AAV-shRNA treatment and were euthanized at 6 months after vector administration. (A) Collagen deposition and collagen fibers were examined by Masson's trichrome and Sirius red staining of liver sections, respectively. Masson staining and Sirius Red staining were observed by light microscopy. Sirius Red staining was also observed by polarized optical microscopy.  $\alpha$ -SMA was detected by (A) IHC staining and (D) western blotting. Quantification of collagen deposition by (B) Masson staining and (C) Sirius Red staining was performed using Image-Pro Plus software, and ImageJ software v.1.31 was used to quantify  $\alpha$ -SMA in (D) western blotting. Scale bars in Masson and Sirius Red staining, 250  $\mu$ m. Scale bar in IHC of  $\alpha$ -SMA, 20  $\mu$ m. \*\*\* $P$ <0.05. The representative sections are presented. Data of proteins are expressed as the means  $\pm$  SD ( $n=3$ ). AAV, adeno-associated virus; shRNA, short hairpin RNA; HBV, hepatitis B virus;  $\alpha$ -SMA,  $\alpha$ -smooth muscle actin; IHC, immunohistochemical.

To clarify the functional relationships of the identified proteins, a PPI network was created using OmicsBean. In the PPI network, GSTP1, which participated in glutathione metabolism, chemical carcinogenesis, and metabolism of

xenobiotics by cytochrome P450, and ribosomal proteins, including Rpl13, Rpl37, and Rpl27a, were upregulated. Additionally, FABP1, ME1, and ACAA1, which were relevant to the PPAR signaling pathway and metabolic pathways, were

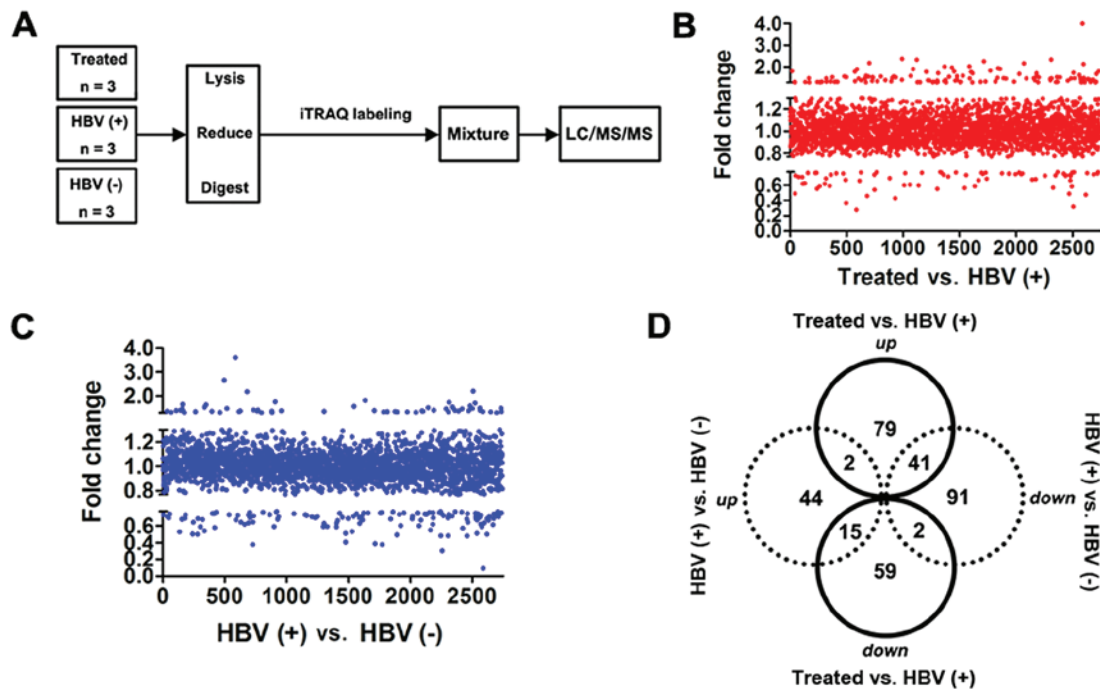


Figure 3. Differentially expressed proteins are identified by the iTRAQ method. (A) Schematic flowchart of the iTRAQ method. Total proteins were identified in the treated, (B) HBV(+) and (C) HBV(-) groups. Each point indicates one protein in B and C. (D) Up- and downregulated proteins were identified, and fold changes >1.3 are depicted in Venn-Euler diagrams. iTRAQ, isobaric tags for relative and absolute quantitation; HBV, hepatitis B virus.

downregulated in the treatment group compared with that in HBV(+) mice (Figs. 4D and S2B).

*Verification of proteins associated with oxidative stress and the PPAR signaling pathway by western blotting.* In order to identify the therapeutic mechanisms of liver fibrosis by AAV-shRNA treatment, we next focused on differentially expressed proteins related to oxidative stress, the PPAR signaling pathway, lipid metabolism, and inflammation, which are involved in hepatic fibrosis. In fact, in our previous study, oxidative stress was revealed to play an important role in liver fibrosis (45). Additionally, differentially expressed proteins related to oxidative stress, including GSTP1 and PRDX1, were identified by iTRAQ-based quantitative proteomics. Thus, in order to verify changes in oxidative stress after treatment, the expression of GSTP1, PRDX1, and TGF- $\beta$ , which are involved in oxidative stress and the redox imbalance, were evaluated by western blotting (Fig. 5). GSTP1 (Fig. 5A) was significantly upregulated in the treated group compared with that in the HBV(+) group (increased 1.57-fold) and was significantly downregulated in HBV(+) mice compared with that in HBV(-) mice (decreased 0.54-fold). PRDX1 (Fig. 5B) and TGF- $\beta$  (Fig. 5C) were significantly downregulated in the treated group compared with that in the HBV(+) group (decreased 0.35-fold and 0.74-fold, respectively) and were upregulated in the HBV(+) group compared with that in the HBV(-) group (increased 3.31-fold and 4.20-fold, respectively). Changes in the expression levels of GSTP1 and PRDX1 verified by western blotting were consistent with the alterations determined by iTRAQ-based quantitative proteomics analysis.

Bioinformatics analysis revealed that the PPAR signaling pathway was activated in the treated group, as demonstrated by downregulation of ACAA1, ME1, and FABP1. Therefore,

the differential expression of these proteins regulated by the PPAR signaling pathway in the liver was next investigated by western blotting. The three proteins were significantly downregulated to 11.90% (ACAA1; Fig. 5D), 42.50% (ME1; Fig. 5E), and 47.10% (FABP1; Fig. 5F) in the treated group compared with that in the HBV(+) group. In a comparison of the HBV(+) with HBV(-) groups, it was determined that the expression levels of ACAA1 and FABP1 were not significantly altered, whereas ME1 was significantly upregulated (increased 1.43-fold; Fig. 5E).

*PPAR- $\gamma$  plays key roles in activating the PPAR signaling pathway.* There are three different isoforms of PPARs, i.e., PPAR- $\alpha$ , PPAR- $\beta/\delta$ , and PPAR- $\gamma$  (56). PPAR- $\alpha$  is mainly expressed in the liver, and PPAR- $\gamma$  is expressed in adipose and liver tissues. Therefore, PPAR- $\alpha$  and PPAR- $\gamma$  expression was evaluated by western blotting. The results revealed that PPAR- $\alpha$  expression was not altered in all three experimental groups. PPAR- $\gamma$  was significantly upregulated by 3.20-fold in the livers of treated mice compared with those of HBV(+) mice; however, no significant changes were observed in the livers of HBV(+) and HBV(-) groups (Fig. 6). These findings suggest that PPAR- $\gamma$  may play an important role inactivating the PPAR signaling pathway following AAV-shRNA treatment and that PPAR- $\alpha$  may not have an important role as PPAR- $\gamma$  in activating the PPAR signaling pathway.

*AAV-shRNA treatment attenuates NF- $\kappa$ B p65 phosphorylation in the liver and decreases IL-6 secretion into the serum.* H&E staining was used to investigate the pathological process of liver fibrosis. Although most hepatocytes appeared histologically normal in all three groups, some hepatic necrosis was observed at 6 months in the HBV(+) mice

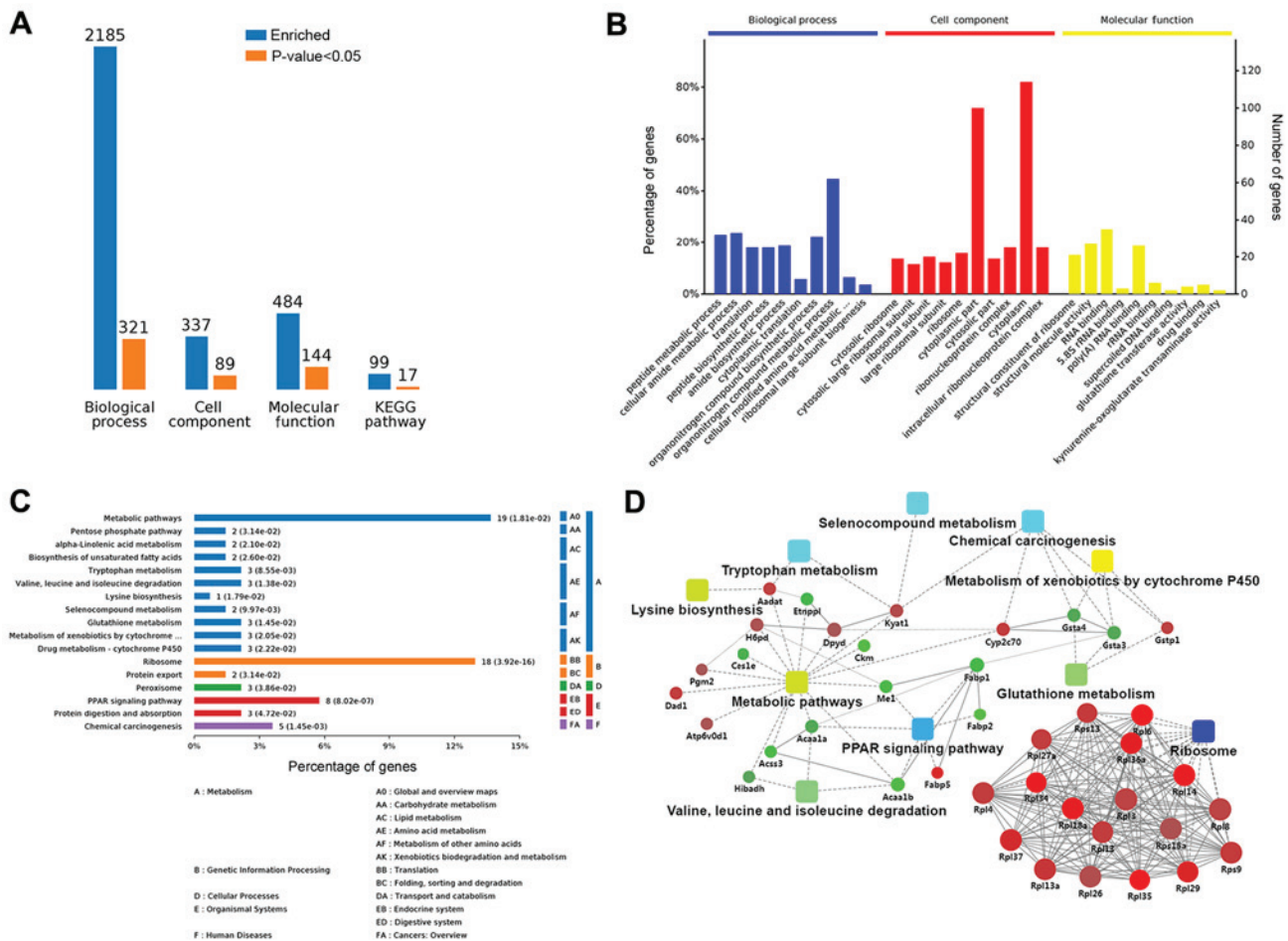


Figure 4. Bioinformatics analysis of the treated group vs. the HBV(+) group. (A) Statistical summary of bioinformatics analysis. (B) Biological processes, cell components, and molecular functions by GO analysis. (C) Global view of the KEGG pathways affected. (D) PPI analysis of differentially expressed proteins. Squares indicate GO/KEGG terms, circles indicate proteins/genes, red circles indicate upregulated proteins, and green circles indicate downregulated proteins. HBV, hepatitis B virus; GO, Gene Ontology; KEGG, Kyoto Encyclopedia of Genes and Genomes; PPI, protein-protein interaction.

(Fig. 7A). NF- $\kappa$ B is a key mediator of inflammatory signaling and plays important roles in liver fibrogenesis (38). Thus, the levels of NF- $\kappa$ B p65 and phosphorylated NF- $\kappa$ B p65 were then examined *in vivo* and *in vitro* using western blotting. The levels of phosphorylated NF- $\kappa$ B p65/NF- $\kappa$ B p65 were significantly reduced in the treatment group compared with that in the HBV(+) group in livers and in LX-2 cells after transfection with pAAV-shRNA; 90.5 and 69% decreases were observed *in vivo* and *in vitro* after treatment, respectively (Fig. 7B, Fig. S3). The expression of the inflammatory factor IL-6 was also measured by ELISA in serum. IL-6 levels in the serum were decreased by over 92% after treatment compared to the HBV (+) group (Fig. 7C).

**Discussion**

Chronic HBV infection is a major health problem in developing countries, including China, and up to one-third of chronically HBV-infected individuals will progress to fibrosis, cirrhosis, and even HCC (57-59). Liver fibrosis involves inflammation induced by a vicious circle of hepatic damage, driving HSC activation and worsening liver damage (9,10). Liver fibrosis is a reversible process that represents the pivotal early stage of hepatic cirrhosis (60), and few therapies for liver fibrosis

have been developed. Thus, it is necessary to elucidate the mechanisms of hepatic fibrosis and develop new medicines for blocking and reversing hepatic fibrosis. Our previous study revealed that AAV-shRNAs had anti-hepatic fibrosis effects in HBV-replicated mice with liver fibrosis (44). Moreover, fibrotic markers, including  $\alpha$ -SMA, collagen I, and III, were significantly reduced. However, the mechanisms mediating the antifibrotic effects of AAV-shRNAs remain unclear. In the present study, ITRAQ-based quantitative proteomics was used to elucidate the antifibrotic mechanism of AAV-shRNAs. Through a comprehensive analysis comparing the treatment group and HBV(+) mice, it was determined that ribosomal proteins, downstream proteins of the PPAR signaling pathway, and inflammation- and oxidative stress-related proteins were significantly enriched in the AAV-shRNA-treated group. In order to elucidate the mechanisms of liver fibrosis, the involvement of oxidative stress, the PPAR signaling pathway, and inflammation, which are closely associated with liver fibrosis, were investigated.

Previously studies have suggested that TGF- $\beta$ , GSTP1, and PRDX1 are correlated with oxidative stress or ROS imbalance (18,61-63). In the present study, it was also determined that these proteins were altered in treated mice compared with that in HBV(+) mice. Numerous studies have demonstrated that

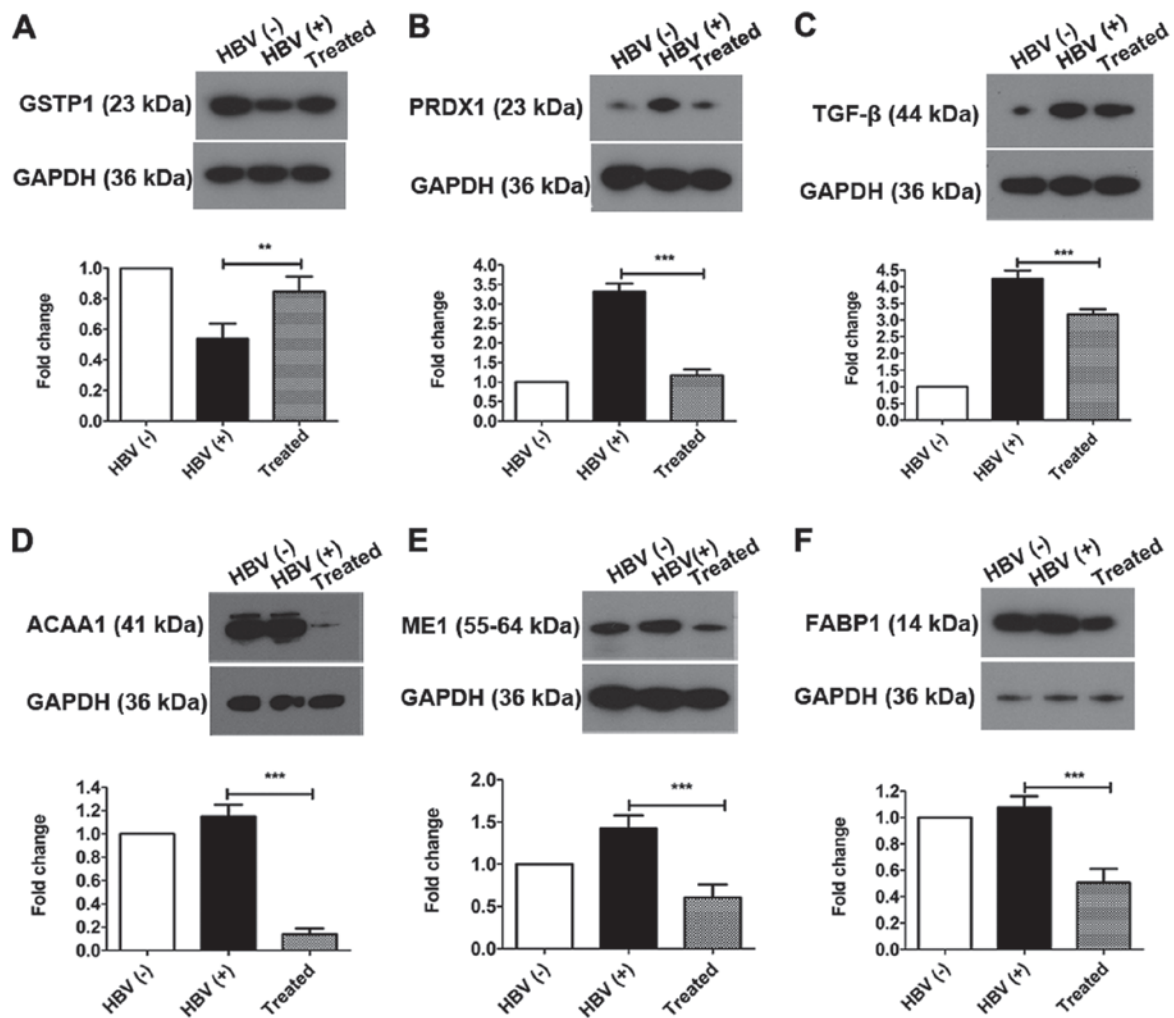


Figure 5. Oxidative stress is alleviated and downstream proteins in the PPAR signaling pathway are altered by AAV-shRNA treatment. The differentially expressed proteins (A) GSTP1, (B) PRDX1 and (C) TGF-β were identified and confirmed by western blotting. Downstream proteins in the PPAR signaling pathway, including (D) ACAA1, (E) ME1 and (F) FABP1, were downregulated in the treated group compared with that in the HBV(+) group. \*\*P<0.01 and \*\*\*P<0.001. Protein data are expressed as the means ± SD (n=3). PPAR, peroxisome proliferator-activated receptor; AAV, adeno-associated virus; shRNA, short hairpin RNA; GSTP1, glutathione S-transferase Pi 1; PRDX1, peroxiredoxin-1; TGF, transforming growth factor; ACAA1, acetyl-CoA acyl-transferase 1; ME1, malic enzyme 1; FABP1, fatty acid binding protein 1; HBV, hepatitis B virus.

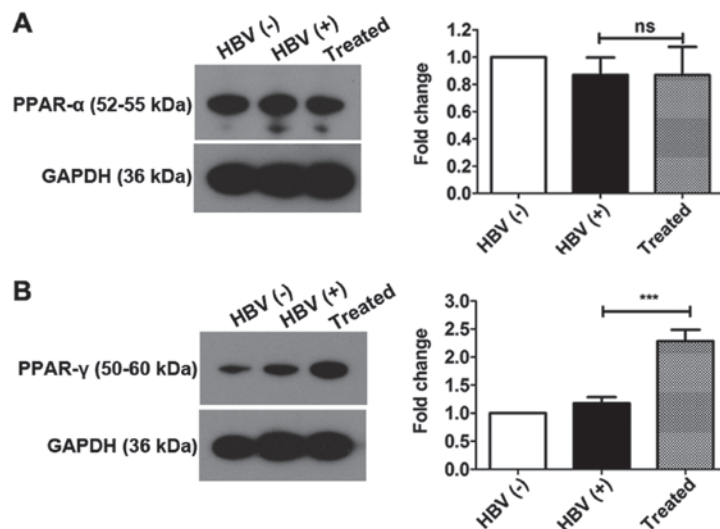


Figure 6. PPAR-γ rather than PPAR-α plays a key role in activating the PPAR signaling pathway. Mice received AAV-shRNA treatment and were sacrificed at 6 months after injection. Total protein was extracted from liver samples. The expression of (A) PPAR-α and (B) PPAR-γ were detected by western blotting. \*\*\*P<0.05. Protein data are expressed as the means ± SD (n=3). PPAR, peroxisome proliferator-activated receptor; AAV, adeno-associated virus; shRNA, short hairpin RNA; ns, not significant.

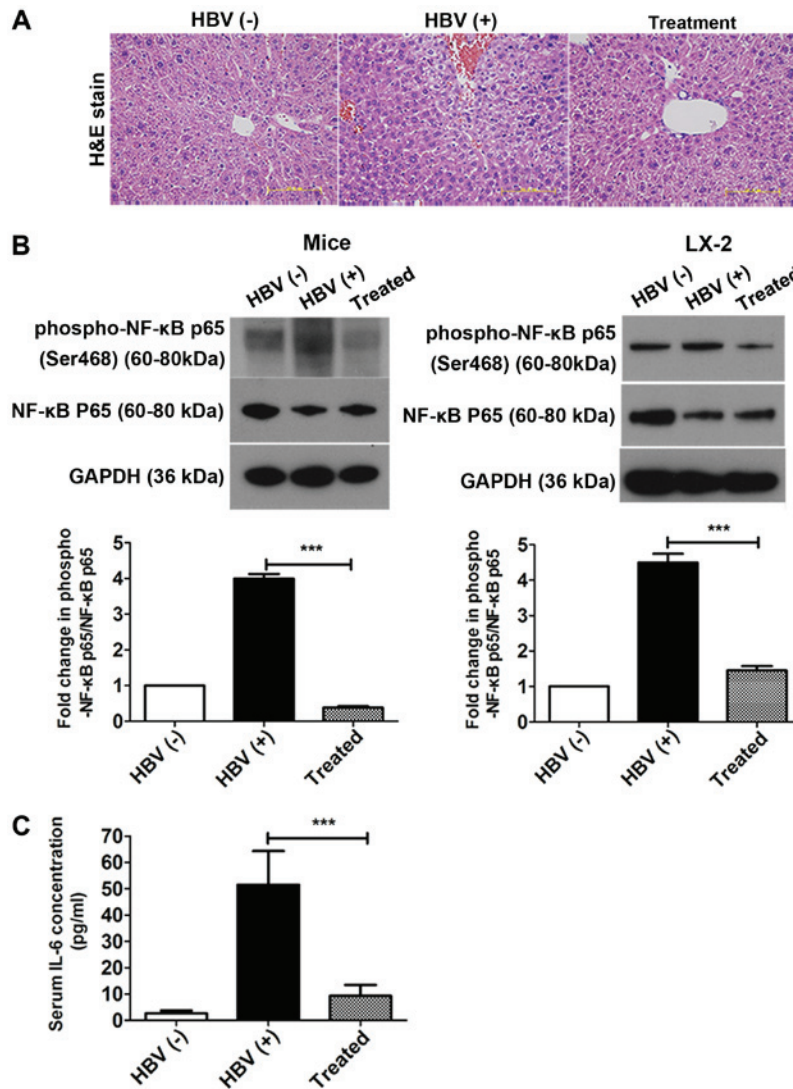


Figure 7. AAV-shRNA treatment improves liver tissue histology and alleviates inflammation by attenuating the NF- $\kappa$ B signaling pathway and reducing serum IL-6 levels. Mice received AAV-shRNA treatment, and liver samples were collected at 6 months after injection. (A) Liver sections stained with H&E. (B) LX-2 cells were transfected with pSSV9-HBV with or without pAAV-shRNA. Phospho-NF- $\kappa$ B (Ser468)/NF- $\kappa$ B p65 levels were evaluated in mice. (C) IL-6 concentrations in serum were determined by ELISA. \*\*\* $P < 0.05$ . Scale bar, 50  $\mu$ m. Data of proteins are expressed as the means  $\pm$  SD ( $n = 3$ ). AAV, adeno-associated virus; shRNA, short hairpin RNA; NF- $\kappa$ B, nuclear factor- $\kappa$ B; IL-6, interleukin-6; H&E, hematoxylin and eosin; ELISA, enzyme linked immunosorbent assay.

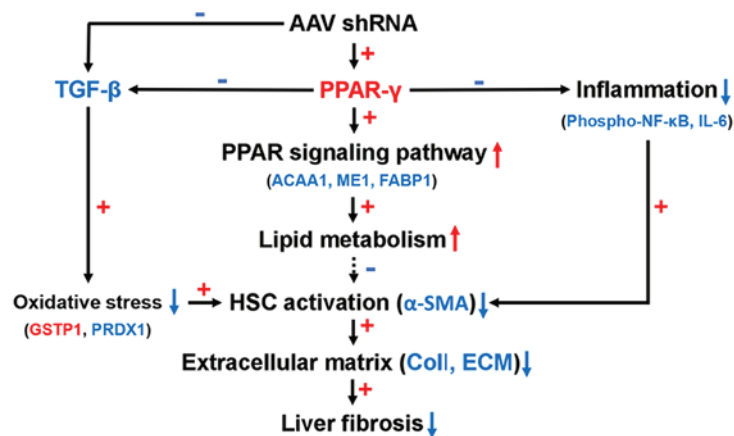


Figure 8. A proposed model showing the mechanism of reduced oxidative stress, inflammation, and PPAR- $\gamma$  signaling activation, resulting in antifibrotic effects of AAV-shRNA treatment. Red color up arrow and plus sign indicate upregulated proteins and positive correlations. Blue color down arrow and minus sign indicate down regulated proteins and negative correlations. AAV, adeno-associated virus; shRNA, short hairpin RNA; PPAR, peroxisome proliferator-activated receptor; TGF, transforming growth factor; NF- $\kappa$ B, nuclear factor- $\kappa$ B; IL-6, interleukin-6; ACAA1, acetyl-CoA acyltransferase 1; ME1, malic enzyme 1; FABP1, fatty acid binding protein 1; GSTP1, glutathione S-transferase Pi 1; PRDX1, peroxiredoxin-1; HSC, hepatic stellate cell;  $\alpha$ -SMA,  $\alpha$ -smooth muscle actin; ECM, extracellular matrix.

TGF- $\beta$  can inhibit the antioxidant system and cause oxidative stress or redox imbalance (5,18,44,64). Additionally, PPAR- $\gamma$  activation can block the TGF- $\beta$  signaling pathway (65). Hence, disruption of TGF- $\beta$  expression can relieve oxidative stress. In the present study, reduction of TGF- $\beta$  expression was observed following treatment with AAV-shRNA-TGF- $\beta$  by direct inhibition of TGF- $\beta$  mRNA at the transcript level, resulting in upregulation of PPAR- $\gamma$ . The findings indicated that AAV-shRNA treatment alleviated oxidative stress by reducing TGF- $\beta$  expression. PRDXs, as redox-regulating proteins, function to eliminate various ROS and maintain cellular redox homeostasis (66). PRDX1 can be easily overoxidized on its catalytically active cysteine upon stimulation with various stimuli (62). PRDX1 was significantly upregulated in HBV(+) mice compared with that in HBV(-) mice and was downregulated after treatment, indicating that oxidative stress was reduced. As an important phase II enzyme, GSTP1 can protect cells from oxidative stress in human cancers (61,67). In accordance with a previous study (61,67), it was determined that GSTP1 was increased to alleviate oxidative stress and played a critical role in antioxidant defense after AAV-shRNA treatment. Collectively, these findings revealed that AAV-shRNA treatment could prevent oxidative stress by suppressing the oxidative stress inducers TGF- $\beta$  and PRDX1 and enhancing GSTP1 expression.

In the PPI network, proteins up- or downstream of the PPAR signaling pathway (including ACAA1, ME1, and FABP1) were found to be regulated, suggesting activation of the PPAR signaling pathway. Notably, FABP1 and ME1 were downregulated in the PPAR signaling pathway, as demonstrated by KEGG analysis. These proteins also played pivotal roles in fatty acid synthesis and transport. ACAA1 is broadly expressed in humans and animals and can catalyze free cholesterol and long-chain fatty acids to synthesize esterified cholesterol (68). ACAA1 is also a marker of  $\beta$ -oxidation (69,70). ME1 is the cytoplasmic component of the NADPH pool and is used by fatty acid synthase as a primary lipogenic enzyme. ME1 is also dysregulated in numerous types of cancers and is involved in tumorigenesis and metastasis (71,72). FABP1 is a liver-specific fatty acid-binding protein with key roles in intracellular metabolism (73). Overexpression of FABP1 significantly promotes hepatocyte fatty acid uptake (74), *de novo* lipogenesis (75), and VLDL secretion (73,76). In addition, knockdown of FABP1 significantly suppressed lipid accumulation in hepatocytes (76) and markedly reduced liver weight and hepatic triacylglycerol accumulation (75). Consistent with previous research (69-72,75,76), it was found that ACAA1, ME1, and FABP1 were downregulated in treated mice compared with that in HBV(+) mice. These results indicated that AAV-shRNA treatment inhibited lipogenesis and improved lipid metabolism. Hepatocyte steatosis was observed in HBV(+) mice, consistent with our previous study (52), and was alleviated after AAV-shRNA treatment (44). These findings suggested that AAV-shRNA alleviated hepatocyte steatosis and liver fibrosis by decreasing hepatocyte fatty acid uptake and *de novo* lipogenesis via attenuation of FABP1 and ME1 expression.

PPAR- $\gamma$  has broad anti-inflammatory effects and plays important roles in controlling fibrogenesis and reducing oxidative stress (31,33,56). The present data indicated that AAV-shRNA activated the PPAR signaling pathway

by upregulating PPAR- $\gamma$  expression directly, resulting in decreased expression of liver fibrosis markers ( $\alpha$ -SMA and ECM) and inflammatory factors (TGF- $\beta$  and IL-6), consistent with previous studies (31,33). Recent investigations have revealed that NF- $\kappa$ B is a crucial mediator of inflammatory signals and that activation of NF- $\kappa$ B promotes liver fibrogenesis (37). Therefore, inhibition of the NF- $\kappa$ B pathway may have therapeutic effects on liver fibrosis. In the present study, it was also revealed that NF- $\kappa$ B p65 phosphorylation was inhibited in treated mice compared with that in HBV(+) mice and in cells transfected with pAAV-shRNA. Overall, these data suggested that AAV-shRNA inhibited liver fibrosis by blocking the NF- $\kappa$ B pathway.

There are some limitations to the present study. On one hand, although proteomics is a powerful technology to identify proteins, combining this method with other analyses such as transcriptomics and metabolomics may increase the significance of proteomics data and eventually aid in elucidating the HBV-induced liver disease in a more systematic manner. On the other hand, although we found that removal of causative factors and direct knockdown of TGF- $\beta$  using short hairpin RNAs are realistic therapeutic strategies, which enhanced the reversibility of liver by regulating the PPAR- $\gamma$  and NF- $\kappa$ B pathways in HBV-induced liver fibrosis in mice, the detailed signaling factors in these pathways and the mechanism of action of these molecules remains unclear. Future and ongoing study will explore the mechanism of anti-fibrosis in liver by using an integrative approach.

Based on these findings, we proposed an antifibrotic model for AAV-shRNA (Fig. 8). AAV-shRNA induced PPAR- $\gamma$  expression and inhibited TGF- $\beta$  expression and NF- $\kappa$ B phosphorylation. TGF- $\beta$  was downregulated after AAV-shRNA treatment in HBV-replicated mice, leading to relief of oxidative stress by upregulation of GSTP1 and downregulation of PRDX1. TGF- $\beta$  was also downregulated due to upregulation of PPAR- $\gamma$ . Upregulation of PPAR- $\gamma$  resulted in activation of the PPAR- $\gamma$  signaling pathway. The PPAR signaling pathway influenced lipid metabolism by decreasing the expression of FABP1 and ME1 and reducing hepatocyte steatosis. Concurrently, upregulation of PPAR- $\gamma$  inhibited inflammation by blocking the NF- $\kappa$ B signaling pathway by decreasing NF- $\kappa$ B p65 phosphorylation.

## Acknowledgements

We would like to thank Professor Jianhua Zheng at the Institute of Pathogen Biology, Chinese Academy of Medical Sciences and Peking Union Medical College for expert advice on proteomics.

## Funding

The present study was supported by a grant to WL and LY from the CAMS Innovation Fund for Medical Sciences (CIFMS; grant no. 2016-I2M-3-020).

## Availability of data and materials

The datasets used during the present study are available from the corresponding author upon reasonable request.

## Authors' contributions

LY and TC contributed equally to this work. LY, WL and CZ conceived and designed the experiments. LY, JC, LS, and TC performed the experiments. LY analyzed the data. LY and WL wrote the manuscript. All authors read and approved the final manuscript.

## Ethics approval and consent to participate

The study of HBV-related liver fibrosis in mice was performed in accordance with the Guide for the Care and Use of Laboratory Animals, which was approved by the Institutional Animal Care and Use Committee of the Chinese Academy of Medical Sciences.

## Patient consent for publication

Not applicable.

## Competing interests

The authors declare that they have no competing interests.

## References

- Ringelhan M, Heikenwalder M and Protzer U: Direct effects of hepatitis B virus-encoded proteins and chronic infection in liver cancer development. *Dig Dis* 31: 138-151, 2013.
- McMahon BJ: The natural history of chronic hepatitis B virus infection. *Hepatology* 49 (5 Suppl): S45-S55, 2009.
- Lin CL and Kao JH: Risk stratification for hepatitis B virus related hepatocellular carcinoma. *J Gastroenterol Hepatol* 28: 10-17, 2013.
- Bonilla Guerrero R and Roberts LR: The role of hepatitis B virus integrations in the pathogenesis of human hepatocellular carcinoma. *J Hepatol* 42: 760-777, 2005.
- Karayiannis P: Hepatitis B virus: Virology, molecular biology, life cycle and intrahepatic spread. *Hepatol Int* 11: 500-508, 2017.
- Poynard T, Mathurin P, Lai CL, Guyader D, Poupon R, Tainturier MH, Myers RP, Munteanu M, Ratziu V, Manns M, *et al*: A comparison of fibrosis progression in chronic liver diseases. *J Hepatol* 38: 257-265, 2003.
- Hernandez-Gea V and Friedman SL: Pathogenesis of liver fibrosis. *Annu Rev Pathol* 6: 425-456, 2011.
- Alkofer B, Lepenne V and Chiche L: Hepatocellular cancer in the non-cirrhotic liver. *J Visc Surg* 148: 3-11, 2011.
- Friedman SL: Mechanisms of hepatic fibrogenesis. *Gastroenterology* 134: 1655-1669, 2008.
- Friedman SL, Roll FJ, Boyles J and Bissell DM: Hepatic lipocytes: The principal collagen-producing cells of normal rat liver. *Proc Natl Acad Sci USA* 82: 8681-8685, 1985.
- Senoo H, Mezaki Y and Fujiwara M: The stellate cell system (vitamin A-storing cell system). *Anat Sci Int* 92: 387-455, 2017.
- Popov Y and Schuppan D: Targeting liver fibrosis: Strategies for development and validation of antifibrotic therapies. *Hepatology* 50: 1294-1306, 2009.
- Gressner AM, Weiskirchen R, Breitkopf K and Dooley S: Roles of TGF- $\beta$  in hepatic fibrosis. *Front Biosci* 7: d793-d807, 2002.
- Rahimi RA and Leof EB: TGF- $\beta$  signaling: A tale of two responses. *J Cell Biochem* 102: 593-608, 2007.
- Shek FW and Benyon RC: How can transforming growth factor  $\beta$  be targeted usefully to combat liver fibrosis? *Eur J Gastroenterol Hepatol* 16: 123-126, 2004.
- Weidinger A and Kozlov AV: Biological activities of reactive oxygen and nitrogen species: Oxidative stress versus signal transduction. *Biomolecules* 5: 472-484, 2015.
- Kim YM and Cho M: Activation of NADPH oxidase subunit NCF4 induces ROS-mediated EMT signaling in HeLa cells. *Cell Signal* 26: 784-796, 2014.
- Schafer FQ and Buettner GR: Redox environment of the cell as viewed through the redox state of the glutathione disulfide/glutathione couple. *Free Radic Biol Med* 30: 1191-1212, 2001.
- Dayer R, Fischer BB, Eggen RI and Lemaire SD: The peroxiredoxin and glutathione peroxidase families in *Chlamydomonas reinhardtii*. *Genetics* 179: 41-57, 2008.
- Wheeler MD, Kono H, Yin M, Nakagami M, Uesugi T, Arteil GE, Gäbele E, Rusyn I, Yamashina S, Froh M, *et al*: The role of kupffer cell oxidant production in early ethanol-induced liver disease. *Free Radic Biol Med* 31: 1544-1549, 2001.
- Issemann I and Green S: Activation of a member of the steroid hormone receptor superfamily by peroxisome proliferators. *Nature* 347: 645-650, 1990.
- Greene ME, Blumberg B, McBride OW, Yi HF, Kronquist K, Kwan K, Hsieh L, Greene G and Nimer SD: Isolation of the human peroxisome proliferator activated receptor gamma cDNA: Expression in hematopoietic cells and chromosomal mapping. *Gene Expr* 4: 281-299, 1995.
- Dreyer C, Krey G, Keller H, Givel F, Helftenbein G and Wahli W: Control of the peroxisomal beta-oxidation pathway by a novel family of nuclear hormone receptors. *Cell* 68: 879-887, 1992.
- Xing G, Zhang L, Zhang L, Heynen T, Yoshikawa T, Smith M, Weiss S and Detera-Wadleigh S: Rat PPAR delta contains a CGG triplet repeat and is prominently expressed in the thalamic nuclei. *Biochem Biophys Res Commun* 217: 1015-1025, 1995.
- Chen F, Law SW and O'Malley BW: Identification of two mPPAR related receptors and evidence for the existence of five subfamily members. *Biochem Biophys Res Commun* 196: 671-677, 1993.
- Xu J, Fu Y and Chen A: Activation of peroxisome proliferator-activated receptor-gamma contributes to the inhibitory effects of curcumin on rat hepatic stellate cell growth. *Am J Physiol Gastrointest Liver Physiol* 285: G20-G30, 2003.
- Ahmadian M, Suh JM, Hah N, Liddle C, Atkins AR, Downes M and Evans RM: PPAR $\gamma$  signaling and metabolism: The good, the bad and the future. *Nat Med* 19: 557-566, 2013.
- Leclercq IA, Da Silva Morais A, Schroyen B, Van Hul N and Geerts A: Insulin resistance in hepatocytes and sinusoidal liver cells: Mechanisms and consequences. *J Hepatol* 47: 142-156, 2007.
- Zhao X, Xue J, Wang XL, Zhang Y, Deng M and Xie ML: Involvement of hepatic peroxisome proliferator-activated receptor  $\alpha/\gamma$  in the therapeutic effect of osthole on high-fat and high-sucrose-induced steatohepatitis in rats. *Int Immunopharmacol* 22: 176-181, 2014.
- Guo YT, Leng XS, Li T, Peng JR, Song SH, Xiong LF and Qin ZZ: Effect of ligand of peroxisome proliferator-activated receptor gamma on the biological characters of hepatic stellate cells. *World J Gastroenterol* 11: 4735-4739, 2005.
- Anty R and Lemoine M: Liver fibrogenesis and metabolic factors. *Clin Res Hepatol Gastroenterol* 35 (Suppl 1): S10-S20, 2011.
- Sun K, Wang Q and Huang XH: PPAR gamma inhibits growth of rat hepatic stellate cells and TGF beta-induced connective tissue growth factor expression. *Acta Pharmacol Sin* 27: 715-723, 2006.
- Yang L, Chan CC, Kwon OS, Liu S, McGhee J, Stimpson SA, Chen LZ, Harrington WW, Symonds WT and Rockey DC: Regulation of peroxisome proliferator-activated receptor-gamma in liver fibrosis. *Am J Physiol Gastrointest Liver Physiol* 291: G902-G911, 2006.
- Brasier AR: The NF- $\kappa$ B regulatory network. *Cardiovasc Toxicol* 6: 111-130, 2006.
- Calzado MA, Bacher S and Schmitz ML: NF- $\kappa$ B inhibitors for the treatment of inflammatory diseases and cancer. *Curr Med Chem* 14: 367-376, 2007.
- Luedde T and Schwabe RF: NF- $\kappa$ B in the liver-linking injury, fibrosis and hepatocellular carcinoma. *Nat Rev Gastroenterol Hepatol* 8: 108-118, 2011.
- Kong D, Zhang F, Wei D, Zhu X, Zhang X, Chen L, Lu Y and Zheng S: Paeonol inhibits hepatic fibrogenesis via disrupting nuclear factor- $\kappa$ B pathway in activated stellate cells: In vivo and in vitro studies. *J Gastroenterol Hepatol* 28: 1223-1233, 2013.
- Liu M, Wu Q, Chen P, Büchele B, Bian M, Dong S, Huang D, Ren C, Zhang Y, Hou X, *et al*: A boswellic acid-containing extract ameliorates schistosomiasis liver granuloma and fibrosis through regulating NF- $\kappa$ B signaling in mice. *PLoS One* 9: e100129, 2014.
- Bromberg J and Wang TC: Inflammation and cancer: IL-6 and STAT3 complete the link. *Cancer Cell* 15: 79-80, 2009.
- Naugler WE and Karin M: The wolf in sheep's clothing: The role of interleukin-6 in immunity, inflammation and cancer. *Trends Mol Med* 14: 109-119, 2008.

41. Wobser H, Dorn C, Weiss TS, Amann T, Bollheimer C, Büttner R, Schölmerich J and Hellerbrand C: Lipid accumulation in hepatocytes induces fibrogenic activation of hepatic stellate cells. *Cell Res* 19: 996-1005, 2009.
42. Montiel-Duarte C, Ansorena E, López-Zabalza MJ, Cenarruzabeitia E and Iraburu MJ: Role of reactive oxygen species, glutathione and NF-kappaB in apoptosis induced by 3,4-methylenedioxyamphetamine ('Ecstasy') on hepatic stellate cells. *Biochem Pharmacol* 67: 1025-1033, 2004.
43. Hernández E, Bucio L, Souza V, Escobar MC, Gómez-Quiroz LE, Farfán B, Kershenovich D and Gutiérrez-Ruiz MC: Pentoxifylline downregulates alpha (I) collagen expression by the inhibition of I-kappaB degradation in liver stellate cells. *Cell Biol Toxicol* 24: 303-314, 2008.
44. Ye L, Kan F, Yan T, Cao J, Zhang L, Wu Z and Li W: Enhanced antiviral and antifibrotic effects of short hairpin RNAs targeting HBV and TGF- $\beta$  in HBV-persistent mice. *Sci Rep* 7: 3860, 2017.
45. Kan F, Ye L, Yan T, Cao J, Zheng J and Li W: Proteomic and transcriptomic studies of HBV-associated liver fibrosis of an AAV-HBV-infected mouse model. *BMC Genomics* 18: 641, 2017.
46. The Gene Ontology Consortium: The gene ontology resource: 20 Years and still GOing strong. *Nucleic Acids Res* 47 (D1): D330-D338, 2019.
47. Kanehisa M, Sato Y, Furumichi M, Morishima K and Tanabe M: New approach for understanding genome variations in KEGG. *Nucleic Acids Res* 47 (D1): D590-D595, 2019.
48. Dillon ST, Bhasin MK, Feng X, Koh DW and Daoud SS: Quantitative proteomic analysis in HCV-induced HCC reveals sets of proteins with potential significance for racial disparity. *J Transl Med* 11: 239, 2013.
49. Kanehisa M and Goto S: KEGG: Kyoto encyclopedia of genes and genomes. *Nucleic Acids Res* 28: 27-30, 2000.
50. Yin L, Qi Y, Xu Y, Xu L, Han X, Tao X, Song S and Peng J: Dioscin inhibits HSC-T6 cell migration via adjusting SDC-4 expression: Insights from iTRAQ-based quantitative proteomics. *Front Pharmacol* 8: 665, 2017.
51. Wiese S, Reidegeld KA, Meyer HE and Warscheid B: Protein labeling by iTRAQ: A new tool for quantitative mass spectrometry in proteome research. *Proteomics* 7: 340-350, 2007.
52. Ye L, Yu H, Li C, Hirsch ML, Zhang L, Samulski RJ, Li W and Niu Z: Adeno-associated virus vector mediated delivery of the HBV genome induces chronic hepatitis B virus infection and liver fibrosis in mice. *PLoS One* 10: e0130052, 2015.
53. Wang X, Li Y, Xu G, Liu M, Xue L, Liu L, Hu S, Zhang Y, Nie Y, Liang S, *et al*: Mechanism study of peptide GMBP1 and its receptor GRP78 in modulating gastric cancer MDR by iTRAQ-based proteomic analysis. *BMC Cancer* 15: 358, 2015.
54. Gan CS, Chong PK, Pham TK and Wright PC: Technical, experimental, and biological variations in isobaric tags for relative and absolute quantitation (iTRAQ). *J Proteome Res* 6: 821-827, 2007.
55. Ashburner M, Ball CA, Blake JA, Botstein D, Butler H, Cherry JM, Davis AP, Dolinski K, Dwight SS, Eppig JT, *et al*: Gene ontology: Tool for the unification of biology. The gene ontology consortium. *Nat Genet* 25: 25-29, 2000.
56. Desvergne B and Wahli W: Peroxisome proliferator-activated receptors: Nuclear control of metabolism. *Endocr Rev* 20: 649-688, 1999.
57. Venook AP, Papandreou C, Furuse J and de Guevara LL: The incidence and epidemiology of hepatocellular carcinoma: A global and regional perspective. *Oncologist* 15 (Suppl 4): S5-S13, 2010.
58. Wang D, Cai H, Yu WB and Yu L: Identification of hepatitis B virus X gene variants between hepatocellular carcinoma tissues and pericarcinoma liver tissues in Eastern China. *Int J Clin Exp Pathol* 7: 5988-5996, 2014.
59. Ringelhan M, O'Connor T, Protzer U and Heikenwalder M: The direct and indirect roles of HBV in liver cancer: Prospective markers for HCC screening and potential therapeutic targets. *J Pathol* 235: 355-367, 2015.
60. Atta HM: Reversibility and heritability of liver fibrosis: Implications for research and therapy. *World J Gastroenterol* 21: 5138-5148, 2015.
61. Li T, Zhao XP, Wang LY, Gao S, Zhao J, Fan YC and Wang K: Glutathione S-transferase P1 correlated with oxidative stress in hepatocellular carcinoma. *Int J Med Sci* 10: 683-690, 2013.
62. Ding C, Fan X and Wu G: Peroxiredoxin 1-an antioxidant enzyme in cancer. *J Cell Mol Med* 21: 193-202, 2017.
63. Ginguay A, Cynober L, Curis E and Nicolis I: Ornithine aminotransferase, an important glutamate-metabolizing enzyme at the crossroads of multiple metabolic pathways. *Biology (Basel)* 6: 18, 2017.
64. Chávez E, Castro-Sánchez L, Shibayama M, Tsutsumi V, Moreno MG and Muriel P: Sulfasalazine prevents the increase in TGF- $\beta$ , COX-2, nuclear NFkB translocation and fibrosis in CCl4-induced liver cirrhosis in the rat. *Hum Exp Toxicol* 31: 913-920, 2012.
65. Bitencourt S, de Mesquita FC, Caberlon E, da Silva GV, Basso BS, Ferreira GA and de Oliveira JR: Capsaicin induces de-differentiation of activated hepatic stellate cell. *Biochem Cell Biol* 90: 683-690, 2012.
66. Rhee SG, Chae HZ and Kim K: Peroxiredoxins: A historical overview and speculative preview of novel mechanisms and emerging concepts in cell signaling. *Free Radic Biol Med* 38: 1543-1552, 2005.
67. Halliwell B: Oxidative stress and cancer: Have we moved forward? *Biochem J* 401: 1-11, 2007.
68. Reza JZ, Doosti M, Salehipour M, Packnejad M, Mojarrad M and Heidari M: Modulation peroxisome proliferators activated receptor alpha (PPAR alpha) and acyl coenzyme A: Cholesterol acyltransferase (ACAT1) gene expression by fatty acids in foam cell. *Lipids Health Dis* 8: 38, 2009.
69. Guo Y, Jolly RA, Halstead BW, Baker TK, Stutz JP, Huffman M, Calley JN, West A, Gao H, Searfoss GH, *et al*: Underlying mechanisms of pharmacology and toxicity of a novel PPAR agonist revealed using rodent and canine hepatocytes. *Toxicol Sci* 96: 294-309, 2007.
70. van der Leij FR, Bloks VW, Grefhorst A, Hoekstra J, Gerding A, Kooi K, Gerbens F, te Meerman G and Kuipers F: Gene expression profiling in livers of mice after acute inhibition of beta-oxidation. *Genomics* 90: 680-689, 2007.
71. Menendez JA and Lupu R: Fatty acid synthase and the lipogenic phenotype in cancer pathogenesis. *Nat Rev Cancer* 7: 763-777, 2007.
72. Murai S, Ando A, Ebara S, Hirayama M, Satomi Y and Hara T: Inhibition of malic enzyme 1 disrupts cellular metabolism and leads to vulnerability in cancer cells in glucose-restricted conditions. *Oncogenesis* 6: e329, 2017.
73. Wang G, Bonkovsky HL, de Lemos A and Burczynski FJ: Recent insights into the biological functions of liver fatty acid binding protein 1. *J Lipid Res* 56: 2238-2247, 2015.
74. Wu YL, Peng XE, Zhu YB, Yan XL, Chen WN and Lin X: Hepatitis B virus X protein induces hepatic steatosis by enhancing the expression of liver fatty acid binding protein. *J Virol* 90: 1729-1740, 2016.
75. Mukai T, Egawa M, Takeuchi T, Yamashita H and Kusudo T: Silencing of FABP1 ameliorates hepatic steatosis, inflammation, and oxidative stress in mice with nonalcoholic fatty liver disease. *FEBS Open Bio* 7: 1009-1016, 2017.
76. Wolfrum C, Buhlmann C, Rolf B, Borchers T and Spener F: Variation of liver-type fatty acid binding protein content in the human hepatoma cell line HepG2 by peroxisome proliferators and antisense RNA affects the rate of fatty acid uptake. *Biochim Biophys Acta* 1437: 194-201, 1999.



This work is licensed under a Creative Commons Attribution-NonCommercial-NoDerivatives 4.0 International (CC BY-NC-ND 4.0) License.